Supplement of Atmos. Chem. Phys., 17, 13605–13624, 2017
https://doi.org/10.5194/acp-17-13605-2017-supplement

Atmospheric Chemistry and Physics
Open Access
EGU

Supplement of

Diurnal and day-to-day characteristics of ambient particle mass size distributions from HR-ToF-AMS measurements at an urban site and a suburban site in Hong Kong

Berto Paul Lee et al.

Correspondence to: Chak Keung Chan (chak.k.chan@cityu.edu.hk)

Text S1. Particle size characterization by HR-AMS

The working principle of the AMS has been described extensively in the literature (Canagaratna et al., 2007;DeCarlo et al., 2006;Drewnick et al., 2005;Jimenez et al., 2003;Jimenez et al., 2007). The particle size acquisition mode (*PToF mode*) relies on aerodynamic sizing as the measurement of particle flight time between two fixed points in space in near vacuum conditions. The incident particle beam passes a rotating double-slit disk, which permits pulses of particles to enter the flight chamber. The chopper operates at a fixed frequency (~150 Hz) and has a duty cycle of 2-4% depending on individual instruments. Recent updates to the instrument design include a different chopper design (ePToF – efficient particle time-of-flight) with a higher particle throughput rate. Data in this study originate from instruments of the older conventional PToF design and is also the basis for following discussion.

The acceleration of a particle into the vacuum interior of the AMS is a function of its size (Jimenez et al., 2003) and thus particles of different size in the pulse ensemble travel at different velocities which are determined from particle flight times over a fixed flight path (i.e. the length of the chamber). Ions arriving at the detector are counted as a function of time between two subsequent particle packages passing through the particle chopper slit. Averaging over several chopper cycles yields a distribution of ions with respect to particle size and enables the measurement of mass concentrations of specific ions as a function of particle size, or of specific bulk species (Organics, SO4, NO3, NH4, Chl) by employing the fragmentation table as in the unit mass resolution acquisition mode (*V-mode*).

Primary logged data in PToF mode is the particle flight time from which velocity is directly inferred due to the fixed flight path length. Velocity can be related to particle diameter by calibration with a set of particles of known size. AMS sizing takes place in near vacuum conditions with particles subject to the free molecular flow regime rather than the transition regime, and consequently AMS size distributions are reported in terms of vacuum-aerodynamic diameter. The relationship between electrical mobility (D_m) and vacuum-aerodynamic diameter (D_{va}) is given by (Jayne et al., 2000):

$$D_{va} = D_m \times \delta_p \times S \qquad \text{Eq. (1)}$$

where δ_p is the particle density and S a particle shape factor for non-spherical particles or those with internal voids. S has been experimentally determined for nitrate (S=0.8). For most other particles, where information on the shape factor are unknown, particles are assumed spherical (S=1). DeCarlo et al. provide a more fundamental discussion of the relationships of different particle diameters and their relation to particle density (DeCarlo et al., 2004;Slowik et al., 2004). Particle size calibrations for the AMS instrument in this study were carried out pre- and post-campaign with sets of monodisperse polystyrene latex particles (PSL, Duke Scientific, CA) in the range of 80nm to 800nm (at least 8 individual particle sizes per calibration). To compensate for the slow evaporation of PSL, the vaporizer temperature was temporarily increased to 800°C from its default value of 600°C for the duration of the calibration. As PSL ion flight traces (m/z 104) are typically broad, the particle flight time was chosen as the leading edge rather than apex of the signal trace, with an addition of half a chopper width time (*0.5*duty cycle/chopper frequency*) to account for chopper broadening. D_{va} in nm and particle velocity v in m/s calculated from the fixed chamber length and measured flight times are related empirically by the following equation (Jayne et al., 2000):

$$v = v_l + \frac{v_g - v_l}{1 + \left(\frac{D_{va}}{D^*}\right)^b} \quad \text{Eq. (2)}$$

where v_l is the gas velocity inside the aerodynamic lens, v_g the velocity of the gas as it leaves the lens, D_{va} the vacuum aerodynamic diameter calculated from the PSL particle diameter and the PSL density of 1.05 g/cm^3 and a shape factor of 1. D* and b are empirical parameters without concrete physical meaning. As per calibration only particle velocity v and vacuum aerodynamic diameter D_{va} are known. The remaining parameters are determined by a non-linear curve fit of v against D_{va} using the relationship describe by Eq. (2).

Text S2. Treatment of PToF data

Standard AMS data treatment procedures were employed for the integration of the ion signals in SQUIRREL for unit-mass resolution data (*V-mode and PToF mode*) and PIKA for high resolution data (*W-mode*).

While in V- and W-mode, ions signals from particle constituents are inferred from the difference of blocked (gas-phase ion signals) and unblocked (sum of gas-phase and particle-phase ion signals) particle beam mass spectra, the baseline in the PToF mode for each m/z in the acquisition range is established by averaging of the ion signal in two defined time regions (DC markers) at the very beginning and very end of the chopper cycle. These correspond to velocities of particles beyond the upper and lower transmission capability of the instrument and can therefore represent background ion contributions (Allan et al., 2003).

In m/z channels where gas-phase species may interfere with the first DC marker region (e.g. m/z 15 or m/z 44), only the second DC marker is used for the PToF baseline. In this work, DC markers for all m/z ratios in the range of 12 – 150 were checked individually to determine the most appropriate selection of DC markers for each m/z channel. Mass concentrations per PToF mode run are calculated by application of the quantification principles of the unit-mass resolution mode (*V-mode*) with additional corrections for the chopper frequency and slit width to account for the lower number of particles passing into the flight chamber. As the chopping of the particle beam lowers overall sensitivity, the integrated particle mass concentration for each PToF run was normalized to the V-mode concentration of the same time step. To remove any remaining background biases, ambient size distributions in this study were background-corrected by subtraction of the size distributions acquired during particle-free time periods (ambient air sampled through HEPA-filter bypass).

For the evaluation of longer term trends in size distributions, the original AMS mass size distributions at 10min resolution were averaged to 24h distributions (from 00:00 to 23:59 each day) to evaluate progressive change in particle size distributions (“day-to-day“) beyond diurnal influences. Regular reoccurring trends, i.e. diurnal variations, were in turn examined by grouping size distributions by their hour time stamp and reconstructing representative size distributions from the average, median, 25th and 75th percentile of each size bin for each hour of the day.

Lognormal peaks were fitted to each 24h and hour-of-day AMS mass size distribution respectively employing the *Multipeak Fit V2* algorithm in *Igor Pro (Wavemetrics)* using a simple vertical offset as the baseline and initial guesses on peak position, height, and width based on visual inspection of the raw size distribution. The multipeak fitting tool employs the Levenberg-Marquardt algorithm (Gill et al., 1981) as a non-linear least squares fit and iteratively adjusts the initial fit parameter guesses until a convergent solution with minimized residuals is achieved. In sporadic cases, the fitted solution led to excessive deviations from the initial guesses with greatly shifted peak locations and large fluctuations in peak width. In such cases, results from the peak fits of immediately adjacent size distributions (i.e. previous and next distributions in the sequence) were evaluated and used to adjust the fitting process by fixing either the location (*primary*) or the width of the peak (*secondary*) to the average value of the two adjacent fitted distributions. For the diurnal size distributions, measurement data from time periods with large differences in species concentration levels were pooled together. The averaging of mass (or volume) based size distribution involves different uncertainties for each size bin due to the cubic relationship between particle mass (or volume) and particle diameter and the corresponding improvement in signal-to-noise ratio with increasing particle size. To establish reliable diurnal trends we adopt an approach similar to the analysis of conventional species concentration diurnal trends by evaluating size distributions reconstructed from the average, median, 25^{th} and 75^{th} percentile of each size bin. Similar diurnal trends in the fitting parameters across these different size distributions would confirm that changes were indeed recurrent daily while divergent trends would indicate that irregular processes (e.g. episodic events) were more significant in determining size distribution characteristics. Since episodic pollution events and clean periods (e.g. prolonged precipitation) were not removed from the dataset, the quantitative analysis focuses on trends observed in the median dataset to minimize skewing effects of high and low concentration periods.

Uncertainties can arise from the peak fitting process itself. While the bimodality of the size distributions was obvious in most cases (i.e. a main mode with a shoulder towards smaller particle sizes, e.g. Fig. S1), accumulation mode particle mass can occasionally dominate the mass size distribution and diminish the Aitken mode. To achieve confidence in the appropriateness of the bimodal fitting we evaluated both unimodal and bimodal peak fits whenever the Aitken to accumulation mode peak ratio was <10% and we depict a representative example below (Fig. S2a. b). The distribution of the fit residuals (Fig. S2c, d) was examined and cumulative probability distributions of the fit residuals compared by the Kolmogorov-Smirnov test (Fig. S2e) to assess whether fit residuals were significantly different at 95% confidence level (CL). It is evident that the bimodal fit performs better at resolving the raw size distribution in the smaller size region and overall yields a more normal residual distribution. The Kolmogorov-Smirnov test confirms that the residual distributions are statistically different ($D>D_{critical}$ at 95% CL). We tested all borderline cases using the outlined procedure. In this study, bimodal fits yielded unanimously better results in all cases for both diurnal and day-to-day size distributions and all investigated species, i.e. the Aitken mode always remained clearly distinguishable from the accumulation mode.

While the peak fitting algorithm yields a unique individual solution with a set of parameters for which resulting residuals (*difference of fitted and original distribution*) are minimized, the surrounding solution space provides a potentially infinite number of similar solutions with slightly larger residuals. The standard deviations of the fit parameters can provide an estimate of the variability of the peak parameters between the final fit solution and the

surrounding solution space. We evaluated the uncertainty in peak area (i.e. integrated mode particle mass) which represents the combined uncertainty of the peak position, width and height (which altogether directly determine the peak area) for all fitted size distributions in this work.

Fig. S3 depicts the standard deviation of resolved peak area (i.e. integrated mode particle mass concentration) nominally and relative to the peak area for the diurnal size distributions of NO3 at the urban Mong Kok site in summer 2013 and Tables C1-C2 summarize the values of percent standard deviations for all species at both measurement sites respectively. The median datasets, which were used for quantitative discussion for the diurnal size distribution analysis, exhibited particle mass uncertainties of 14-48% in the Aitken mode and 1-12% in the accumulation mode at the suburban HKUST site, and 7-44% in the Aitken mode and 1-6% in the accumulation mode at the urban MK site. Figure S4 depicts the 75th percentile-bin diurnal variation of NO3 (which displayed the largest uncertainties in Fig. S3) with the corresponding peak area variability, and shows that the interpretation of the diurnal variation would remain largely unaffected from the incurred uncertainties.

For the day-to-day 24h size distributions a corresponding analysis was undertaken, with Fig. S5 depicting the size distributions of NO3 at the HKUST site for all covered seasons exemplarily, and Table S3 summarizes the values of percent standard deviations for all species at both measurement sites respectively. Peak fit uncertainties typically increase with decreasing integrated peak area and can exceed the values of the peak area in the Aitken mode in a small number of cases (e.g. Fig. S5c,e – ratios >1). Quantification of the Aitken mode may not be possible at high levels of confidence in these isolated cases. They were retained in the dataset due to their low frequency of occurrence and to enable a complete discussion over the full concentration range without biasing towards larger concentration (i.e. fitted peak areas) values.

Tables

Table S1. Percentiles of relative standard deviation (*rows; corresponding to the box-whiskers plot in Fig. S3e,f*) in percent from lognormal peak fits (bimodal deconvolution) for the resolved (a) Aitken mode and (b) accumulation mode particle concentration for diurnal size distributions at the HKUST supersite (2011/12), *columns* describe the data set, i.e. reconstructed size distributions from the 25th percentile, median, 75th percentile and mean of the size bins
Sp=Spring, Su=Summer, Fa=Fall, Wi=Winter

(a)

Aitken mode		25th PC Distr.				Median Distr.				75th PC Distr.				Mean Distr.				Range
% SD		Sp	Su	Fa	Wi	Sp	Su	Fa	Wi	Sp	Su	Fa	Wi	Sp	Su	Fa	Wi	
NO3 (UST)	PC-90	67	76	39	85	76	44	54	55	80	75	56	39	36	77	44	42	36-85
	PC-75	52	42	28	57	66	32	39	40	61	59	44	29	22	38	35	34	22-66
	PC-50	**36**	**33**	**22**	**46**	**44**	**26**	**31**	**22**	**40**	**43**	**34**	**23**	**18**	**28**	**24**	**30**	**18-46**
	PC-25	29	25	16	28	26	14	24	18	25	29	22	17	14	19	20	25	14-29
	PC-10	21	20	15	24	19	12	19	15	17	19	17	10	13	13	15	21	10-24
SO4 (UST)	PC-90	38	38	42	74	19	36	39	43	22	40	40	42	19	36	37	81	19-81
	PC-75	35	33	38	55	18	28	33	32	18	30	35	64	17	30	30	66	17-66
	PC-50	**28**	**30**	**33**	**32**	**16**	**26**	**27**	**25**	**14**	**24**	**27**	**27**	**14**	**24**	**26**	**48**	**14-48**
	PC-25	21	25	26	24	13	21	22	21	11	18	24	22	12	21	23	40	11-40
	PC-10	17	23	24	19	11	20	20	13	10	14	20	19	10	19	22	35	10-35
Org (UST)	PC-90	52	23	41	44	42	28	32	27	47	48	45	53	46	29	24	32	23-53
	PC-75	41	18	26	28	30	22	27	22	26	39	35	44	36	23	21	25	18-44
	PC-50	**26**	**14**	**17**	**21**	**19**	**18**	**21**	**17**	**20**	**32**	**26**	**35**	**23**	**18**	**19**	**21**	**14-35**
	PC-25	16	11	13	18	17	16	19	15	18	28	20	29	18	14	16	17	11-29
	PC-10	9	9	10	11	14	9	15	12	15	20	17	21	17	11	14	16	9-21

(b)

Accum. mode		25th PC Distr.				Median Distr.				75th PC Distr.				Mean Distr.				Range
% SD		Sp	Su	Fa	Wi	Sp	Su	Fa	Wi	Sp	Su	Fa	Wi	Sp	Su	Fa	Wi	
NO3 (UST)	PC-90	8	5	8	4	7	5	6	3	4	9	6	3	3	4	5	1	1-9
	PC-75	6	4	7	3	3	4	5	2	4	7	5	2	2	3	5	1	1-7
	PC-50	**4**	**3**	**5**	**2**	**3**	**3**	**5**	**2**	**3**	**4**	**5**	**2**	**2**	**3**	**4**	**1**	**1-5**
	PC-25	3	3	4	2	2	3	4	1	3	3	4	2	2	2	4	1	1-4
	PC-10	2	2	4	1	2	2	4	1	2	2	3	1	2	2	3	1	1-4
SO4 (UST)	PC-90	2	3	3	5	2	2	2	3	3	2	3	4	2	2	2	2	2-5
	PC-75	2	2	2	2	2	2	2	2	2	2	2	3	1	2	2	2	1-3
	PC-50	**2**	**2**	**2**	**1**	**2**	**2**	**2**	**2**	**2**	**2**	**2**	**2**	**1**	**2**	**2**	**1**	**1-2**
	PC-25	2	2	2	1	1	2	2	1	1	2	2	2	1	2	2	1	1-2
	PC-10	1	2	1	1	1	2	2	1	1	1	2	1	1	2	2	1	1-2
Org (UST)	PC-90	29	12	16	9	18	8	9	5	10	6	7	3	18	7	5	5	3-29
	PC-75	18	9	11	7	10	5	5	3	6	4	5	2	11	5	4	3	2-18
	PC-50	**12**	**7**	**5**	**5**	**6**	**4**	**4**	**3**	**4**	**3**	**4**	**2**	**7**	**3**	**3**	**3**	**2-12**
	PC-25	7	4	3	3	5	3	3	2	3	2	3	2	5	2	2	2	2-7
	PC-10	4	4	1	2	4	2	2	1	2	2	2	1	2	1	2	2	1-4

Table S2. Percentiles of relative standard deviation (*rows; corresponding to the box-whiskers plot in Fig. S3e,f*) in percent from lognormal peak fits (bimodal deconvolution) for the resolved (a) Aitken mode and (b) accumulation mode particle concentration for diurnal size distributions at the urban MK site (2013), *columns* describe the data set, i.e. reconstructed size distributions from the 25th percentile, median, 75th percentile and mean of the size bins
Sp=Spring, Su=Summer

(a)

Aitken mode % SD		25th PC Distr. Sp	25th PC Distr. Su	Median Distr. Sp	Median Distr. Su	75th PC Distr. Sp	75th PC Distr. Su	Mean Distr. Sp	Mean Distr. Su	Range
NO3 (MK)	PC-90	38	46	40	34	40	41	22	26	22-46
	PC-75	27	34	26	28	34	35	20	16	16-35
	PC-50	**15**	**24**	**23**	**21**	**25**	**28**	**18**	**14**	**14-28**
	PC-25	9	20	19	17	18	22	15	12	9-22
	PC-10	6	19	16	14	15	20	13	11	6-20
SO4 (MK)	PC-90	63	46	35	38	24	31	23	21	21-63
	PC-75	50	36	30	36	21	28	21	20	20-50
	PC-50	**44**	**33**	**28**	**24**	**20**	**23**	**19**	**18**	**18-44**
	PC-25	37	27	24	21	17	20	15	17	15-37
	PC-10	33	25	21	19	15	18	15	16	15-33
Org (MK)	PC-90	22	12	22	19	30	21	15	14	12-30
	PC-75	16	10	12	12	18	11	12	8	8-18
	PC-50	**10**	**8**	**10**	**9**	**10**	**9**	**8**	**7**	**7-10**
	PC-25	8	7	8	7	7	8	6	6	6-8
	PC-10	7	6	7	6	6	6	5	5	5-7

(b)

Accum. mode % SD		25th PC Distr. Sp	25th PC Distr. Su	Median Distr. Sp	Median Distr. Su	75th PC Distr. Sp	75th PC Distr. Su	Mean Distr. Sp	Mean Distr. Su	Range
NO3 (MK)	PC-90	9	9	6	7	3	5	2	5	2-9
	PC-75	6	8	4	5	3	4	2	4	2-8
	PC-50	**4**	**6**	**3**	**4**	**2**	**3**	**2**	**3**	**2-6**
	PC-25	2	5	2	4	2	3	1	3	1-5
	PC-10	2	4	1	3	1	3	1	2	1-4
SO4 (MK)	PC-90	4	3	2	3	2	5	2	3	2-5
	PC-75	3	2	2	3	2	4	2	2	2-4
	PC-50	**3**	**2**	**2**	**2**	**1**	**4**	**2**	**2**	**1-4**
	PC-25	2	2	2	2	1	3	1	2	1-3
	PC-10	2	2	1	2	1	3	1	2	1-3
Org (MK)	PC-90	9	8	8	7	9	5	6	6	5-9
	PC-75	6	7	5	5	5	4	5	4	4-7
	PC-50	**5**	**5**	**4**	**4**	**3**	**4**	**3**	**4**	**3-5**
	PC-25	4	4	3	3	3	3	3	3	3-4
	PC-10	2	3	3	3	5	2	2	2	2-3

Table S3. Percentiles of percent standard deviation (*rows; corresponding to the box-whiskers plot in Fig. S5e,f*) from lognormal peak fits (bimodal deconvolution) for the resolved Aitken mode and accumulation mode for 24h day-to-day size distributions at (a) the suburban HKUST site and (b) the urban MK site for all investigated species, *columns* describe the uncertainties in terms of quartiles of resolved peak area, where Q1 refers to the lowest 25% and Q4 the highest 25% of resolved peak area (see also Fig. S4)

(a)

HKUST '11/12 % SD		NO3					SO4					Org				
		Q1	Q2	Q3	Q4	Range	Q1	Q2	Q3	Q4	Range	Q1	Q2	Q3	Q4	Range
Aitken mode	PC-90	95	64	50	27	27-95	97	78	49	30	30-97	62	37	28	26	26-62
	PC-75	58	47	37	24	24-58	91	57	36	20	20-91	41	24	21	22	21-41
	PC-50	**47**	**35**	**25**	**17**	**17-47**	**60**	**39**	**29**	**16**	**16-60**	**30**	**17**	**14**	**17**	**14-30**
	PC-25	30	25	20	13	13-30	32	26	21	13	13-32	25	14	10	12	10-25
	PC-10	20	16	15	8	8-20	24	18	13	11	11-24	16	11	6	7	6-16
Accum. mode	PC-90	31	9	7	4	4-31	4	3	3	3	3-4	18	11	9	7	7-18
	PC-75	13	6	5	3	3-13	3	3	3	2	2-3	9	7	6	5	5-9
	PC-50	**8**	**4**	**3**	**2**	**2-8**	**2**	**2**	**2**	**2**	**~2**	**6**	**4**	**5**	**3**	**3-6**
	PC-25	3	3	2	2	2-3	2	2	2	2	~2	4	3	3	2	2-4
	PC-10	1	2	2	1	1-2	2	2	2	1	1-2	3	2	2	2	2-3

(b)

MK '13 % SD		NO3					SO4					Org				
		Q1	Q2	Q3	Q4	Range	Q1	Q2	Q3	Q4	Range	Q1	Q2	Q3	Q4	Range
Aitken mode	PC-90	62	52	47	30	30-62	94	50	29	24	24-94	23	17	13	16	13-23
	PC-75	41	42	30	25	25-42	47	35	22	16	16-47	16	14	11	12	11-16
	PC-50	**28**	**34**	**21**	**18**	**18-34**	**33**	**24**	**17**	**12**	**12-33**	**11**	**10**	**6**	**8**	**6-11**
	PC-25	21	22	19	12	12-22	26	17	13	9	9-26	8	7	5	6	5-8
	PC-10	6	10	13	8	6-13	19	14	10	5	5-19	6	5	3	3	3-6
Accum. mode	PC-90	22	21	6	6	6-22	7	6	6	4	4-7	13	8	9	8	8-13
	PC-75	17	10	5	3	3-17	4	4	4	2	2-4	8	7	6	4	4-8
	PC-50	**10**	**6**	**4**	**2**	**2-10**	**3**	**2**	**2**	**1**	**1-3**	**6**	**5**	**4**	**2**	**2-6**
	PC-25	6	3	2	2	2-6	2	2	1	1	1-2	4	4	3	2	2-4
	PC-10	3	1	2	1	1-3	1	1	1	1	~1	2	3	2	1	1-3

Table S4. Median organic subcomponent concentrations in NR-PM_1 prior to and during meal hours at the urban MK site and their fractional contribution to total change in Organics in NR-PM_1 (Lee et al., 2015)

Mass conc. μg m^{-3}	Spring				Summer			
	SOA	COA	HOA	Total Org	SOA	COA	HOA	Total Org
Pre-lunch 09:00 – 11:00	3.9	3.0	3.9	10.9	1.6	2.6	2.3	6.5
Lunch 12:00 – 14:00	4.6	7.0	4.0	15.8	1.8	4.0	2.1	8.0
Contribution to ΔTotal Org	+16.3%	+81.4%	+2.3%	---	+18.3%	+94.1%	-8.6%	---
Pre-dinner 15:00 – 17:00	4.4	4.0	3.8	12.1	1.7	3.3	2.3	7.3
Dinner 19:00 – 21:00	4.6	9.2	4.1	17.9	1.6	6.3	2.3	10.1
Contribution to ΔTotal Org	+4.7%	+89.6%	+5.7%	---	-4.4%	+106.3%	-1.9%	---

Table S5. Ratio of 10^{th} and 90^{th} percentile mass concentration to median mass concentration of submicron (NR-PM_1) species at the urban MK site (Lee et al., 2015)

Percentile ratio	Spring			Summer		
	Org	SO4	NO3	Org	SO4	NO3
10^{th} / 50^{th}	0.5	0.3	0.3	0.4	0.3	0.5
90^{th} / 50^{th}	2.1	1.7	2.8	2.3	1.8	2.2

Figures

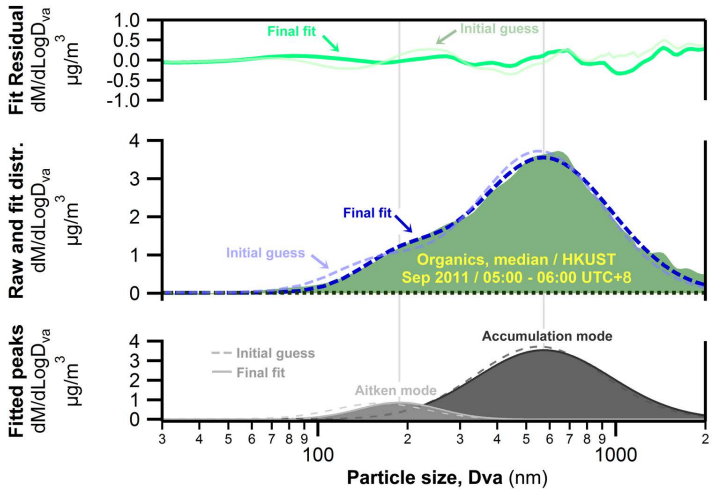

Figure S1. Example of a log-normal peak fit *(Multipeak Fit V2, Igor Pro, Wavemetrics, Levenberg-Marquardt algorithm)* of an AMS organics size distribution

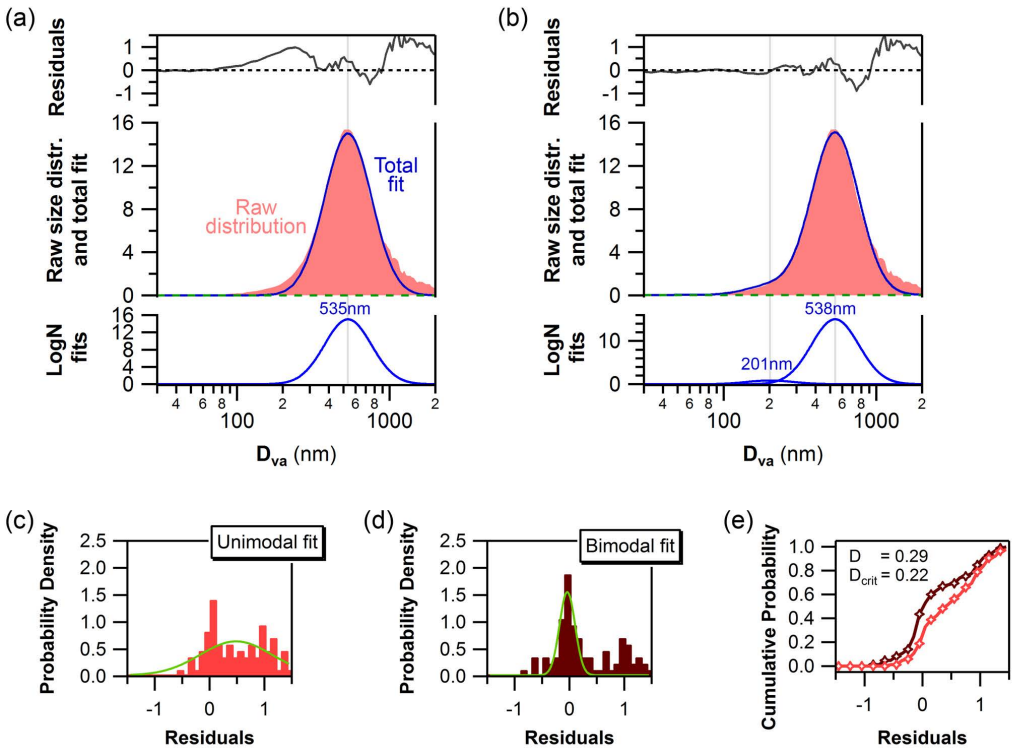

Figure S2. 24h average mass size distribution of sulfate (12/12/2011, suburban HKUST site) with (a) unimodal and (b) bimodal logN peak fitting applied; histograms of residuals from the (c) unimodal and (d) bimodal distributions with Gaussian fit (green); and (e) cumulative probability density functions of uni- and bimodal fit residuals with Kolmogorov-Smirnov D metric values at 95% confidence level

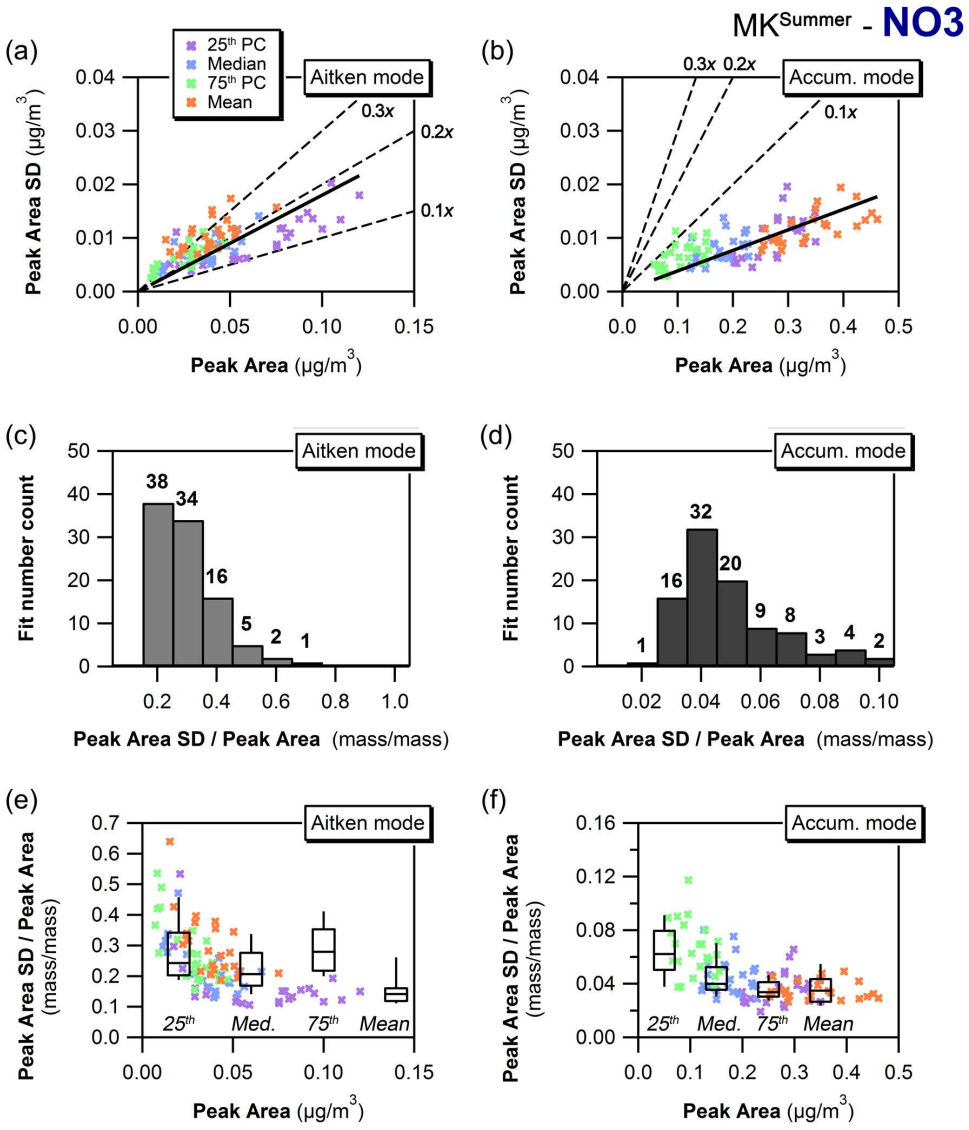

Figure S3. Standard deviation of peak area as a function of mode peak area (a,b), histogram of relative standard deviation i.e. the ratio of standard deviation to mode peak area (c,d) where the last bin also contains all values beyond the last bin range, and relative standard deviation as a function of mode peak area (e,f) for the fitted Aitken and accumulation mode with binned box-whiskers plot (25^{th} to 75^{th} PC box with horizontal median line and 10^{th} to 90^{th} PC whiskers where bins refer to quartiles of peak area from lowest Q1 to highest Q4); data for diurnal size distributions of NO3 at the urban Mong Kok site in summer 2013.

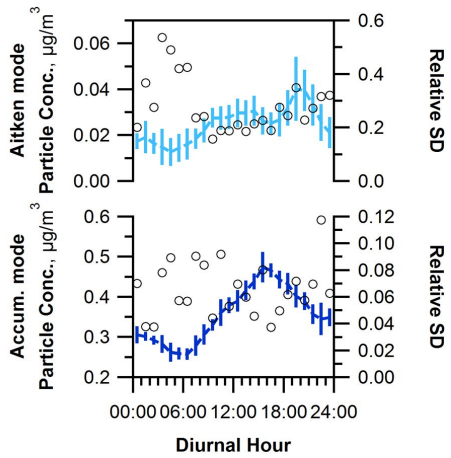

Figure S4. Plot of 75th percentile-bin diurnal variation with peak area fit variability and relative standard deviation (*open circle*), corresponding to green data and second to last box in Fig. S3e,f

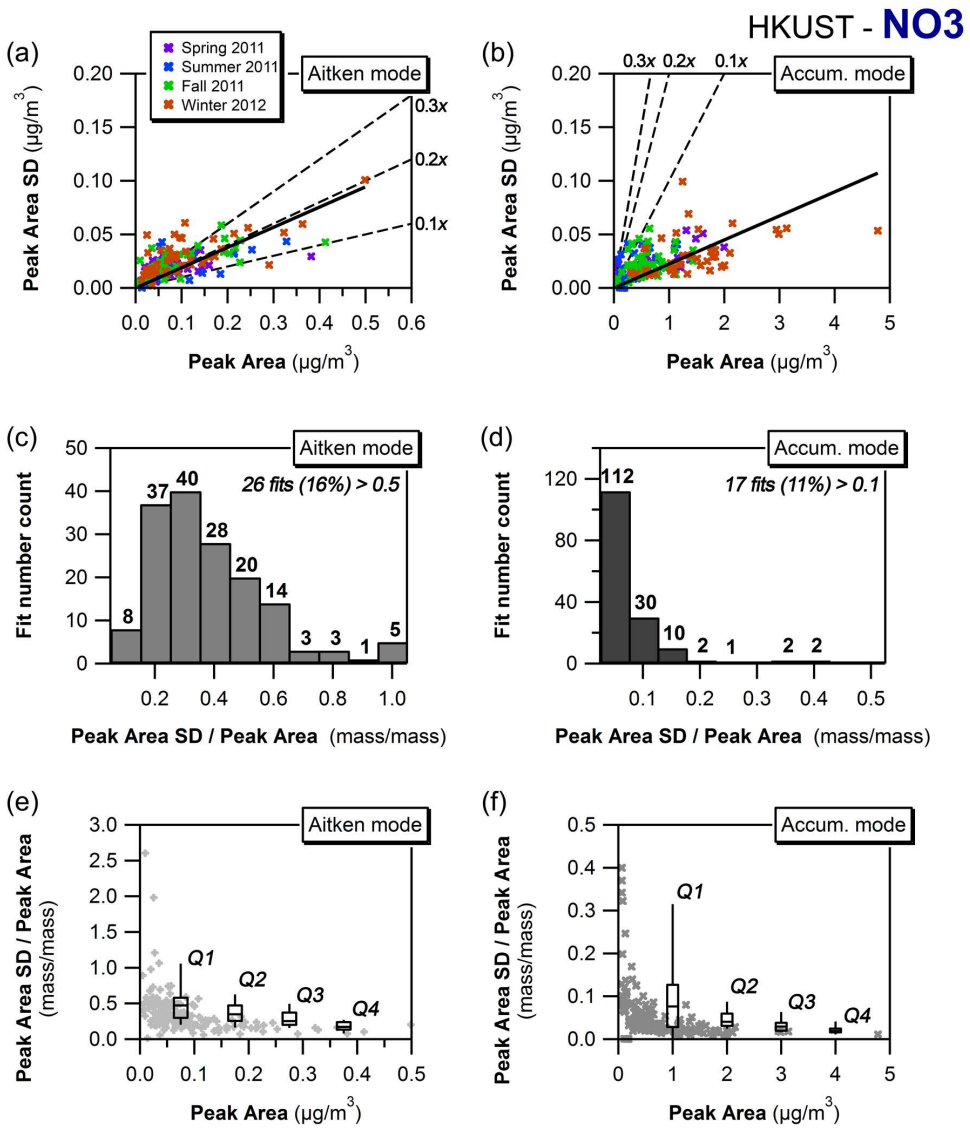

Figure S5. Standard deviation of peak area as a function of mode peak area (a,b), histogram of relative standard deviation i.e. the ratio of standard deviation to mode peak area (c,d) where the last bin also contains all values beyond the last bin range, and relative standard deviation as a function of mode peak area (e,f) for the fitted Aitken and accumulation mode with binned box-whiskers plot (25^{th} to 75^{th} PC box with horizontal median line and 10^{th} to 90^{th} PC whiskers where bins refer to quartiles of peak area from lowest Q1 to highest Q4); data for day-to-day size distributions of NO3 at the HKUST site including all seasons.

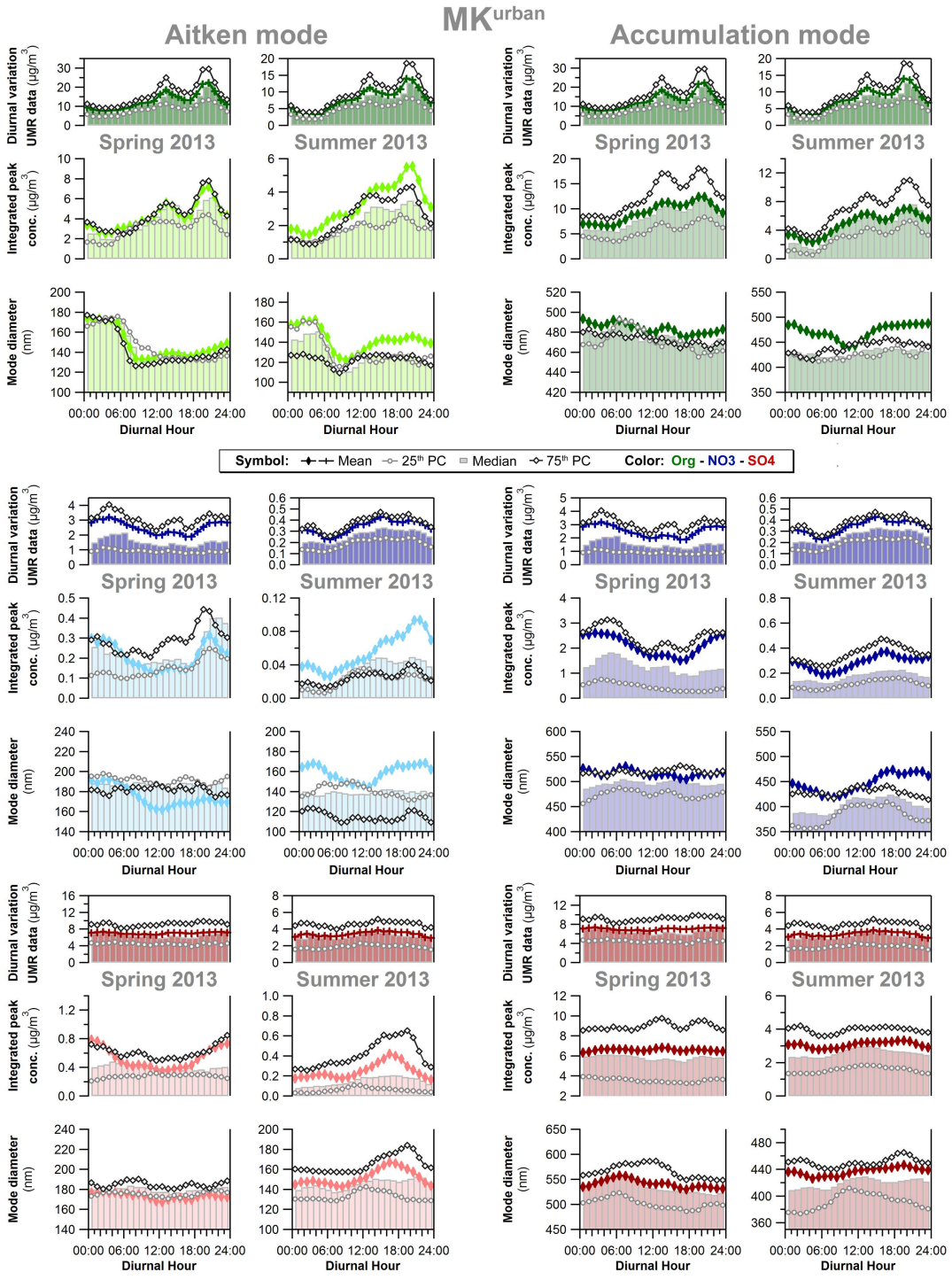

Figure S6. Mode diameter (mass median diameter - MMD), integrated particle mass concentration and width (geometric standard deviation - GSD) of the Aitken mode and accumulation mode from bimodal diurnal peak fits of organic, nitrate and sulfate size distributions at the Mong Kok urban site in spring 2013 and summer 2013; the top panel depicts the diurnal variations of total measured submicron organic, nitrate and sulfate concentrations (AMS V-mode data)

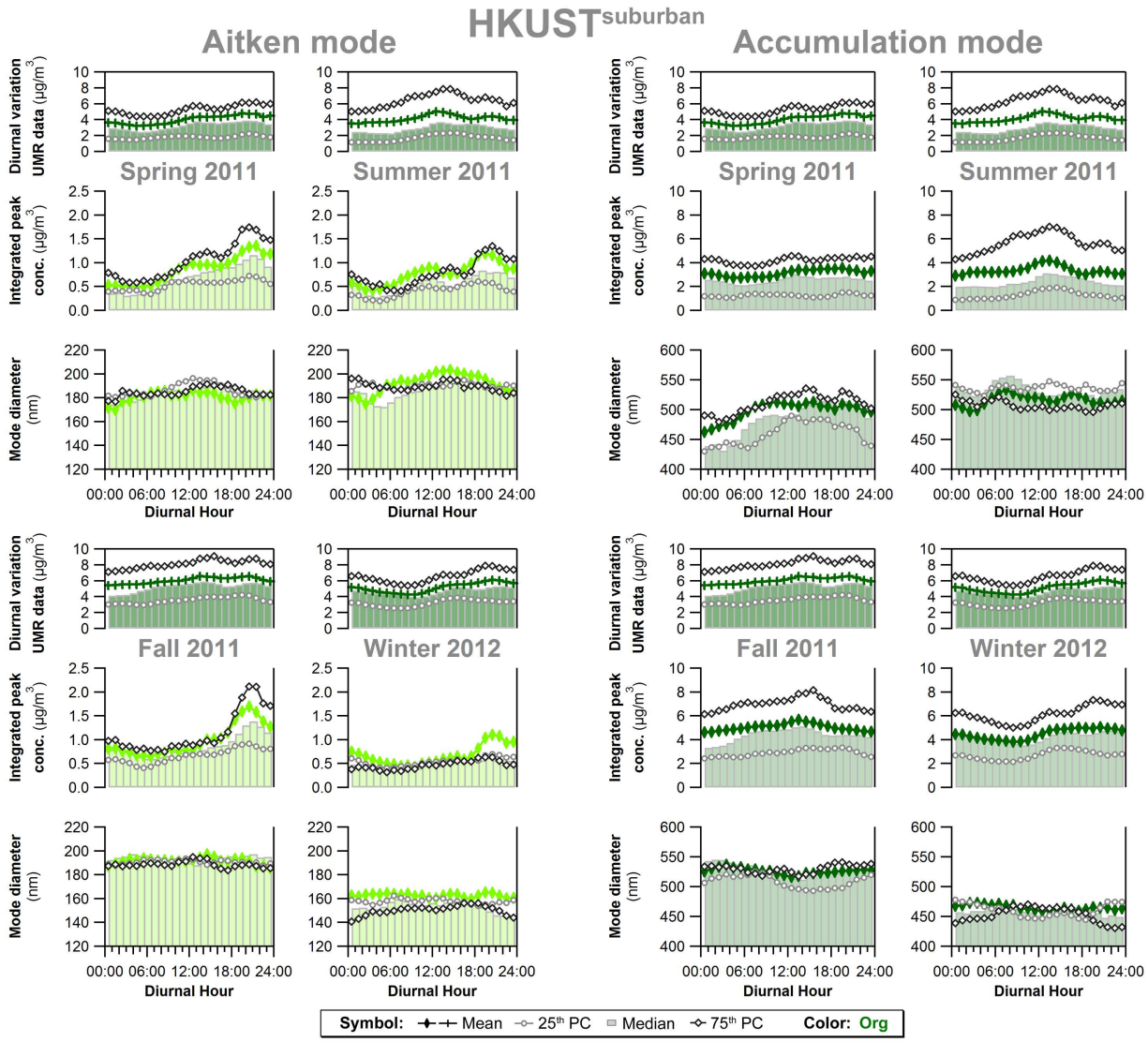

Figure S7. Mode diameter (mass median diameter - MMD), integrated particle mass concentration and width (geometric standard deviation - GSD) of the Aitken mode and accumulation mode from bimodal diurnal peak fits of organic size distributions at the suburban HKUST site in four seasons (May 2011- Feb 2012); the top panel depicts the diurnal variations of total measured submicron organic concentrations (AMS V-mode data)

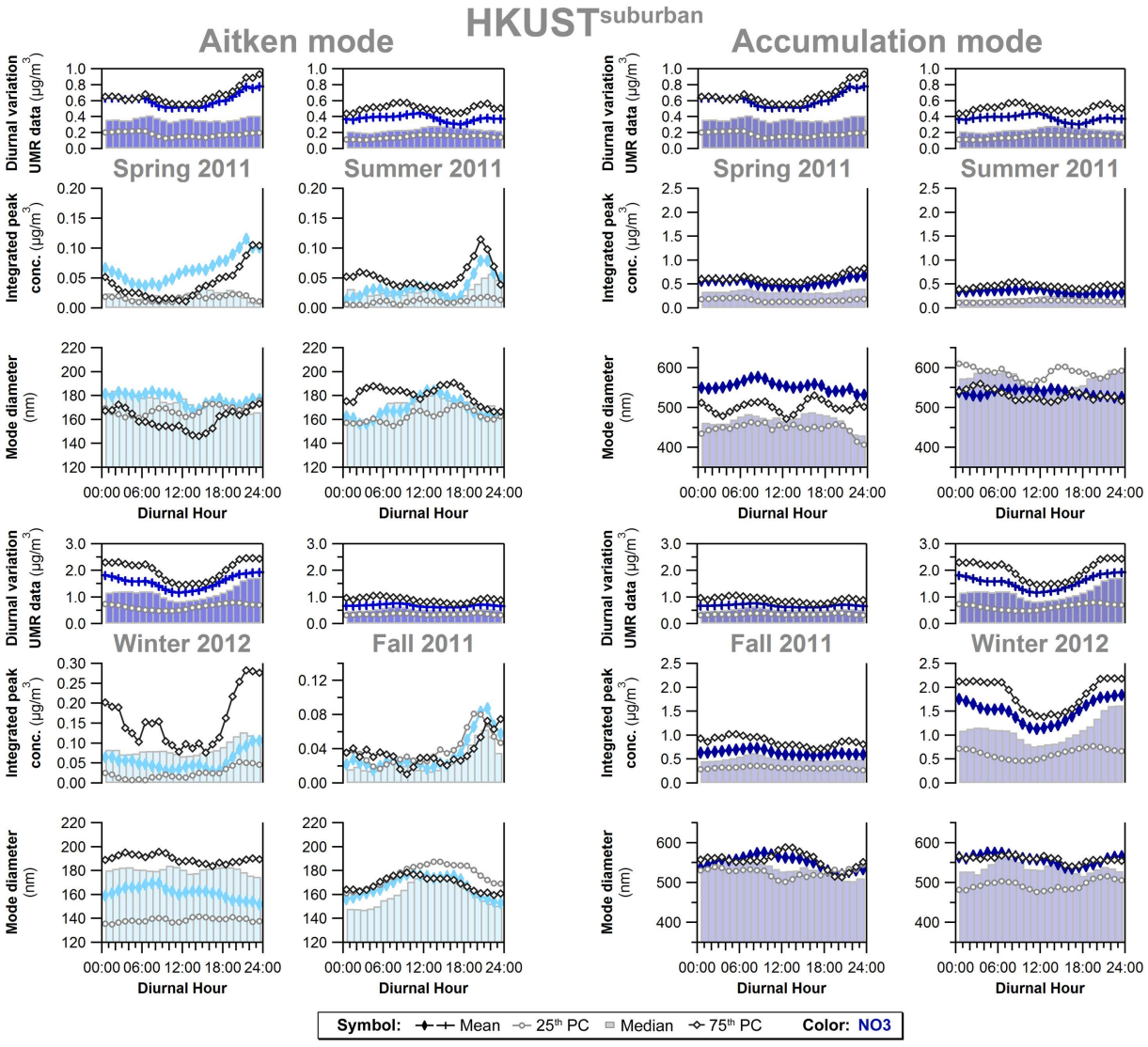

Figure S8. Mode diameter (mass median diameter - MMD), integrated particle mass concentration and width (geometric standard deviation - GSD) of the Aitken mode and accumulation mode from bimodal diurnal peak fits of nitrate size distributions at the suburban HKUST site in four seasons (May 2011- Feb 2012); the top panel depicts the diurnal variations of total measured submicron nitrate concentrations (AMS V-mode data)

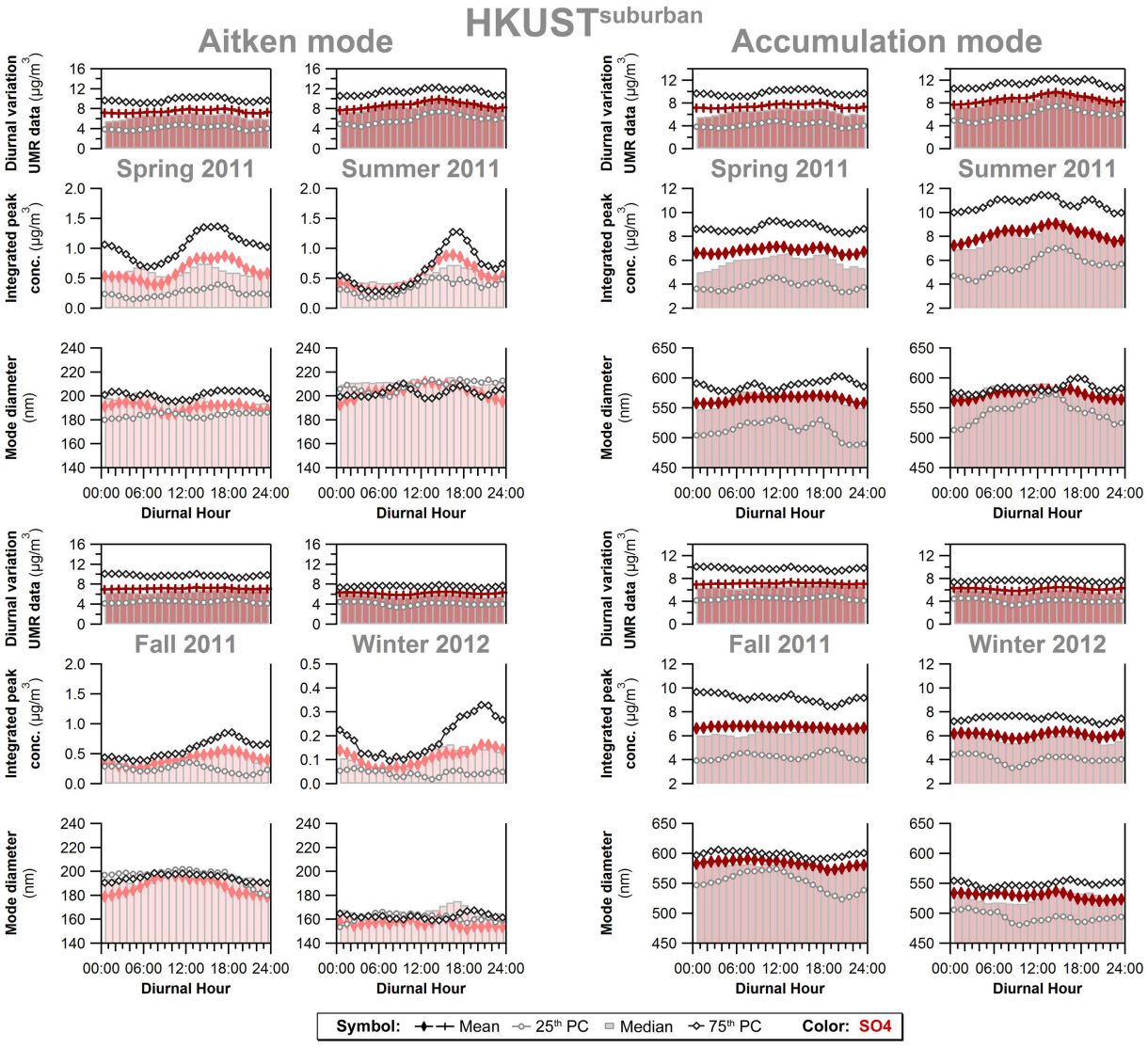

Figure S9. Mode diameter (mass median diameter - MMD), integrated particle mass concentration and width (geometric standard deviation - GSD) of the Aitken mode and accumulation mode from bimodal diurnal peak fits of sulfate size distributions at the suburban HKUST site in four seasons (May 2011- Feb 2012); the top panel depicts the diurnal variations of total measured submicron sulfate concentrations (AMS V-mode data)

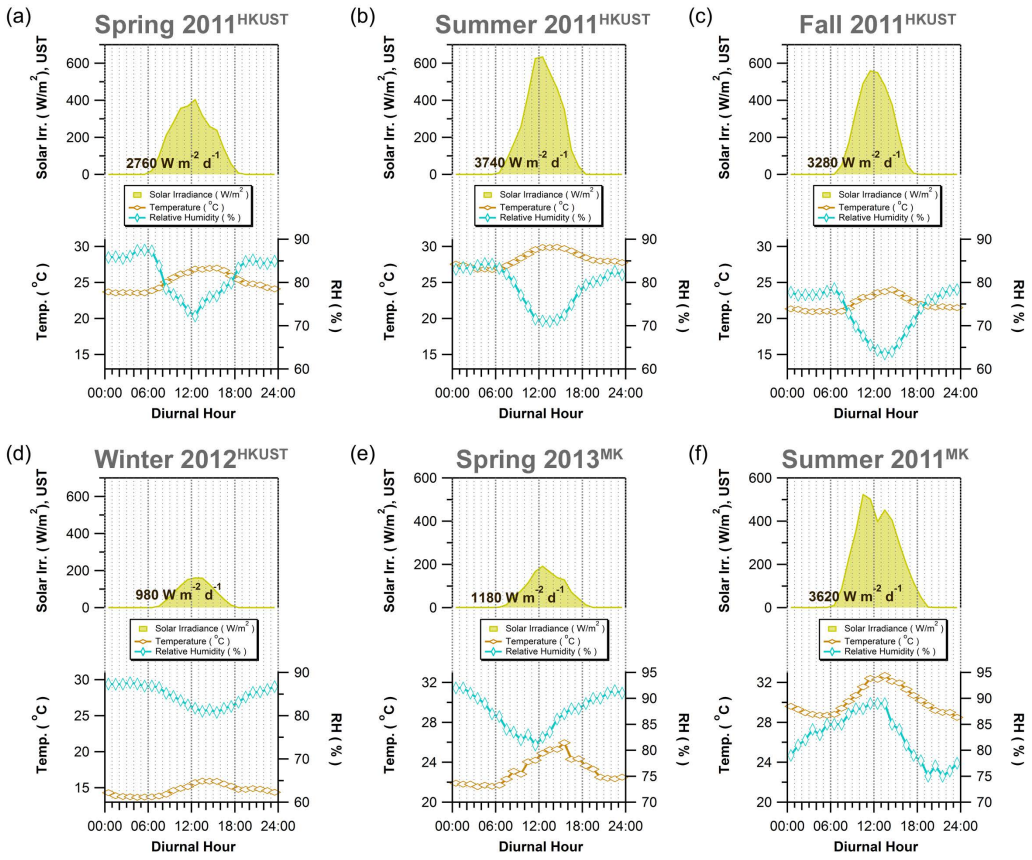

Figure S10. Diurnal variation of temperature (*orange*), RH (*blue*) and solar irradiance (*yellow*) in four seasons in 2011-2012 as well as spring and summer 2013; temperature and RH measurements from the HKUST supersite for the four seasons in 2011-2012, and from the Mong Kok urban site for spring and summer 2013; solar irradiance data from the HKUST supersite in all plots.

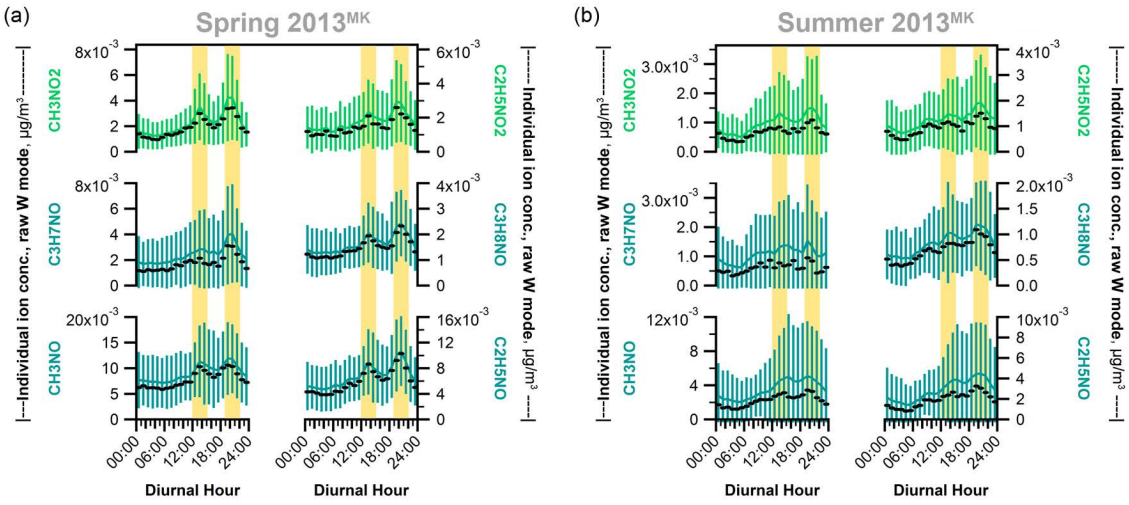

Figure S11. Diurnal variation of fitted $C_xH_yN_zO$ and $C_xH_yN_zO_2$ ions (*raw W-mode mass concentrations*) at the urban Mong Kok site in 2013 in (a) spring and (b) summer, lunch and dinner hours highlighted in yellow

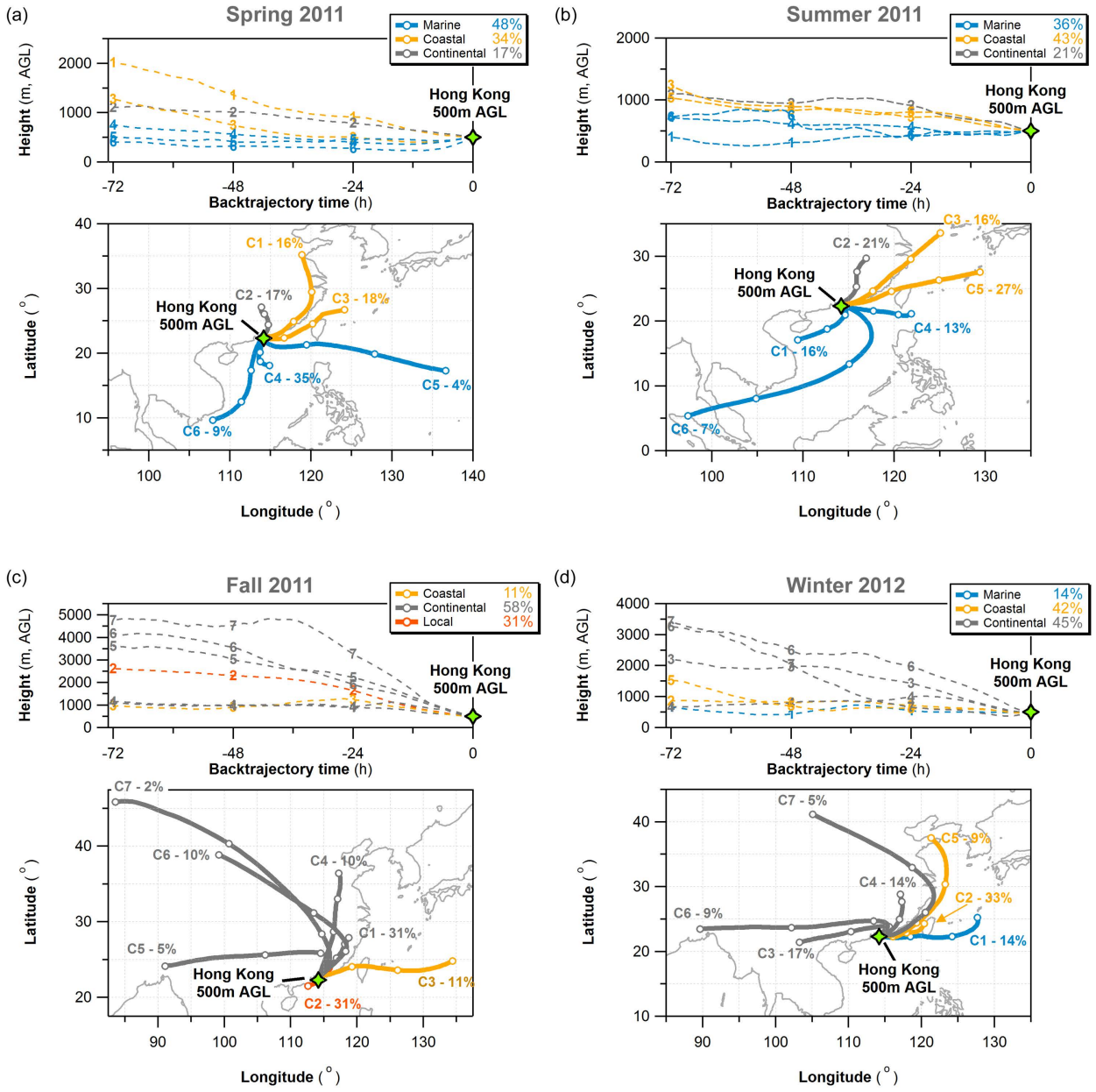

Figure S12. Means of clustered back trajectories (HYSPLIT4, 72h back trajectories) in each sampling season at the suburban HKUST site in (a) spring, (b) summer, (c) fall and (d) winter 2011-2012

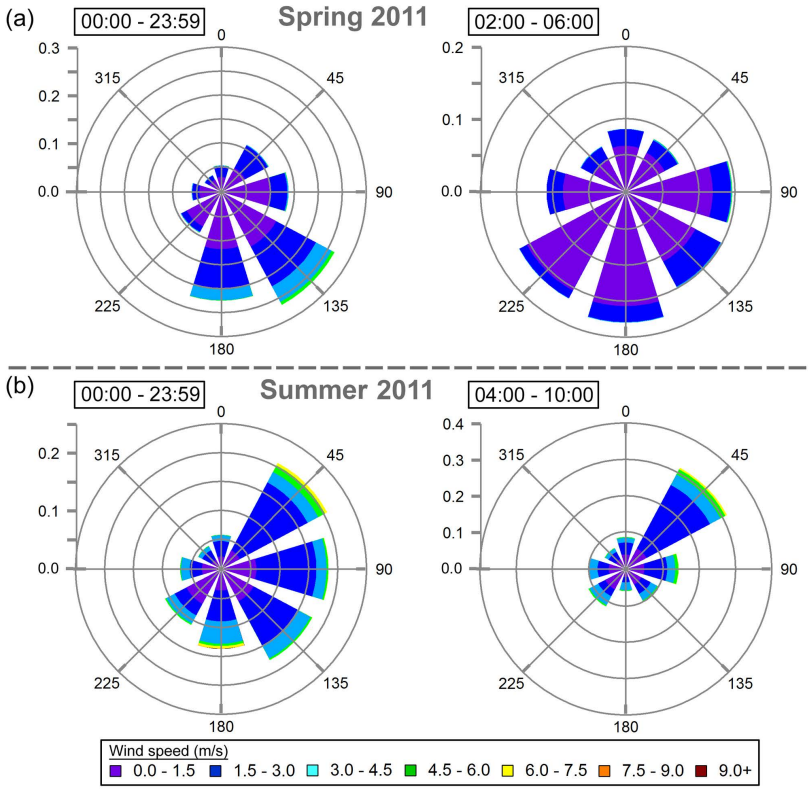

Figure S13. Wind rose plots for observed surface wind frequency at the suburban HKUST site (a) in spring 2011 (2011-05) for the whole sampling period and the nighttime period between 02:00 and 06:00 and (b) in summer 2011 (2011-09) for the whole sampling period and the morning period between 04:00 and 10:00

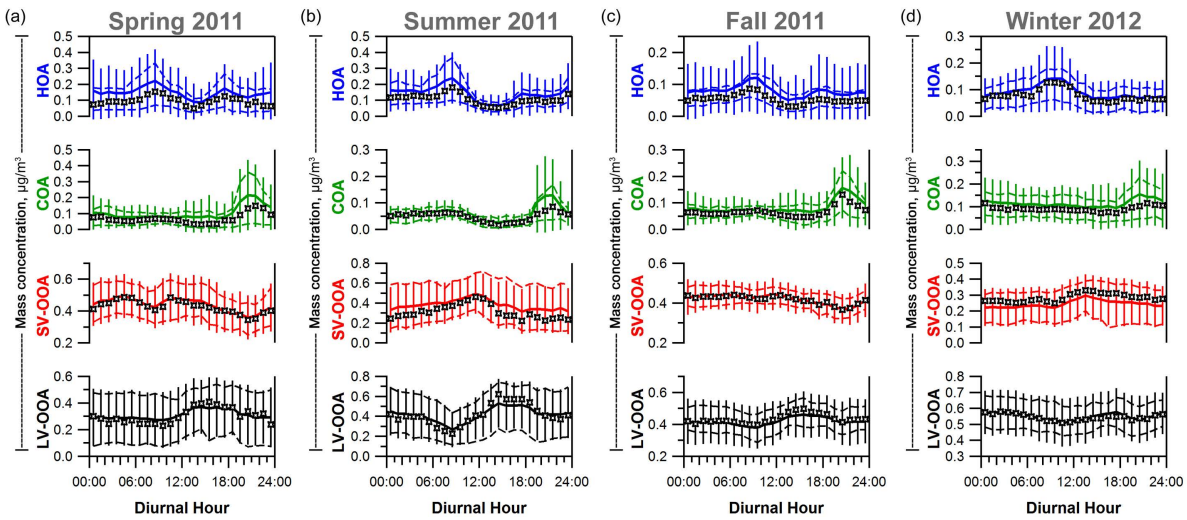

Figure S14. Diurnal variation of PMF-resolved organic aerosol factors at the suburban HKUST site in (a) spring, (b) summer, (c) fall and (d) winter 2011-2012, *mean as colored solid line with standard deviations, median as open markers, 25th and 75th percentiles as hashed colored lines*, for details see Li et al. (Li et al., 2015).

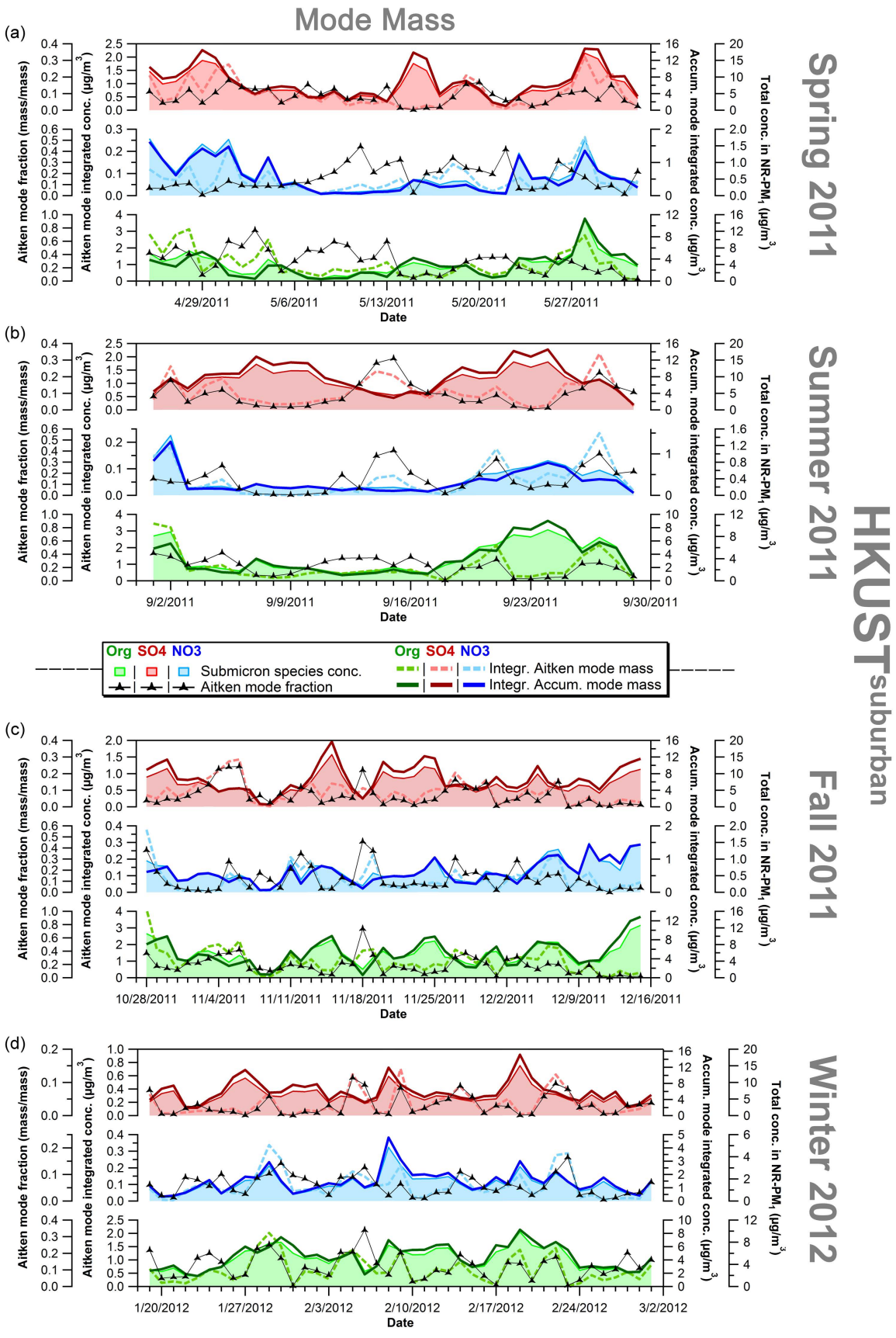
Mode Mass
(a)
(b)
(c)
(d)
Spring 2011
Summer 2011
Fall 2011
Winter 2012
HKUST suburban
Aitken mode fraction (mass/mass)
Aitken mode integrated conc. (μg/m3)
Accum. mode integrated conc. (μg/m3)
Total conc. in NR-PM1 (μg/m3)
Date
4/29/2011
5/6/2011
5/13/2011
5/20/2011
5/27/2011
9/2/2011
9/9/2011
9/16/2011
9/23/2011
9/30/2011
10/28/2011
11/4/2011
11/11/2011
11/18/2011
11/25/2011
12/2/2011
12/9/2011
12/16/2011
1/20/2012
1/27/2012
2/3/2012
2/10/2012
2/17/2012
2/24/2012
3/2/2012
Org SO4 NO3
Submicron species conc.
Aitken mode fraction
Org SO4 NO3
Integr. Aitken mode mass
Integr. Accum. mode mass

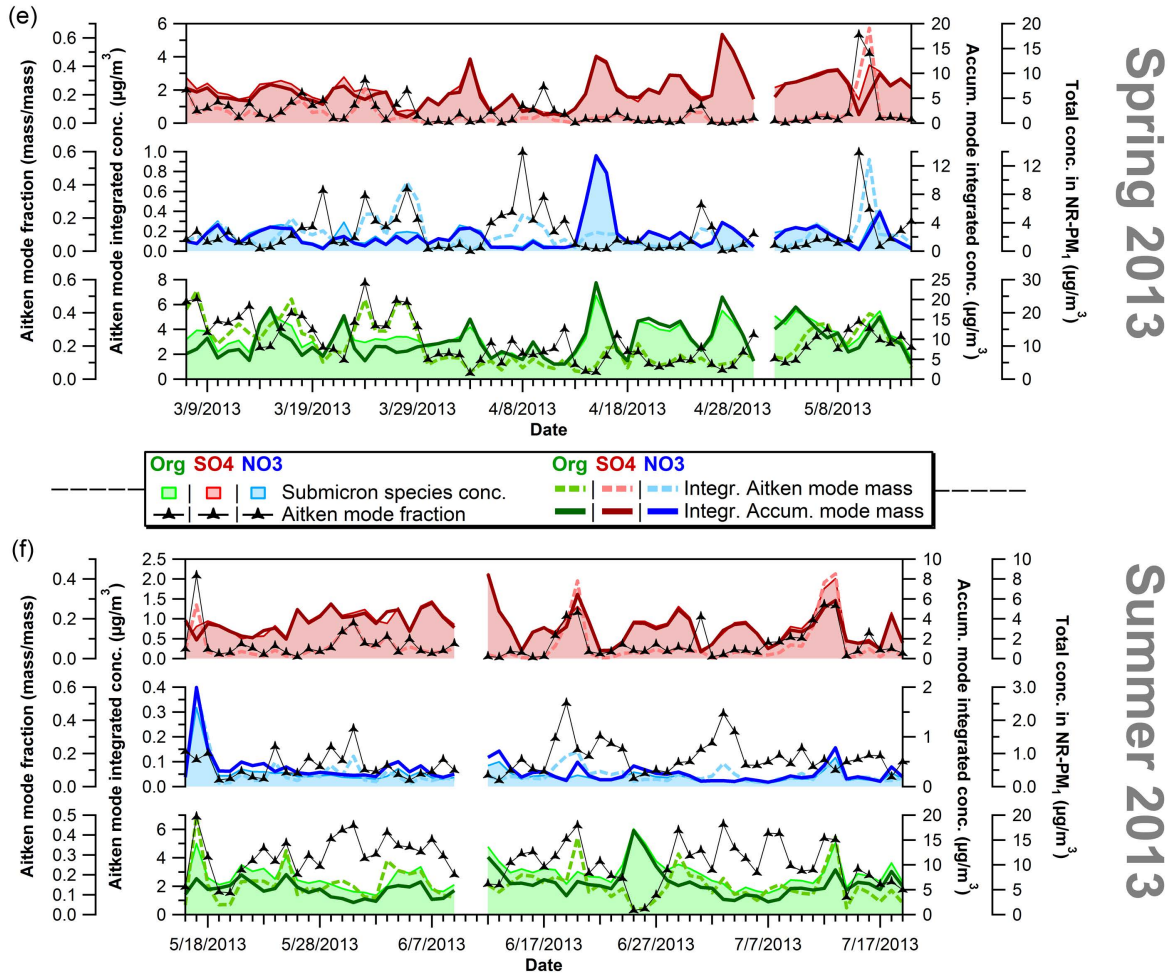

Figure S15. Time series of integrated particle mass concentrations of Aitken and accumulation modes at the suburban HKUST supersite in four seasons in 2011-2012 (a-d) and the urban Mong Kok site in 2013 (e-f), total species mass concentrations are based on V-mode measurements.

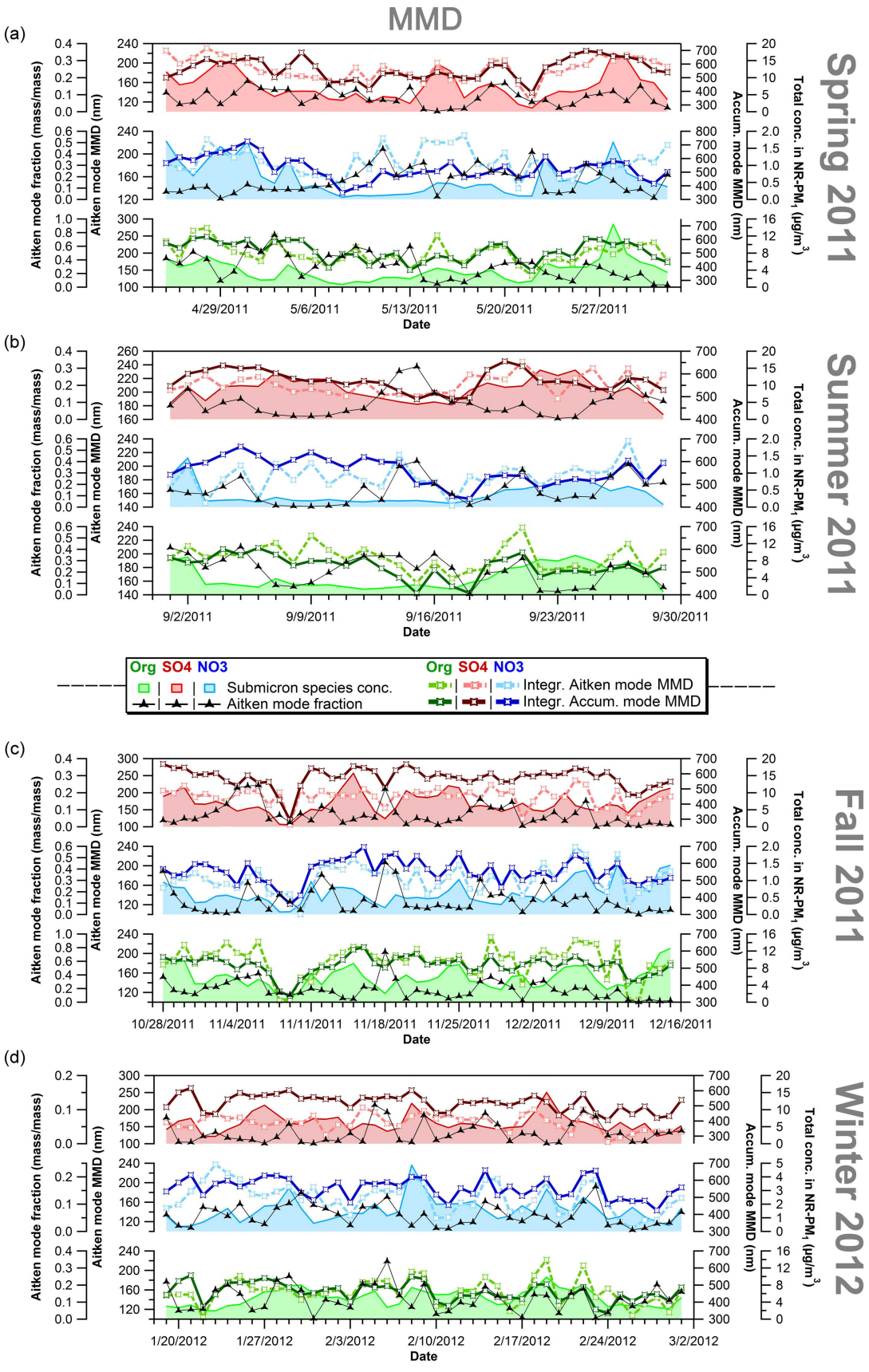
MMD
(a)
Spring 2011
(b)
Summer 2011
HKUSTsuburban
(c)
Fall 2011
(d)
Winter 2012
Aitken mode fraction (mass/mass)
Aitken mode MMD (nm)
Accum. mode MMD (nm)
Total conc. in NR-PM1 (μg/m3)
4/29/2011
5/6/2011
5/13/2011
5/20/2011
5/27/2011
9/2/2011
9/9/2011
9/16/2011
9/23/2011
9/30/2011
10/28/2011
11/4/2011
11/11/2011
11/18/2011
11/25/2011
12/2/2011
12/9/2011
12/16/2011
1/20/2012
1/27/2012
2/3/2012
2/10/2012
2/17/2012
2/24/2012
3/2/2012
Date
Org SO4 NO3
Submicron species conc.
Aitken mode fraction
Org SO4 NO3
Integr. Aitken mode MMD
Integr. Accum. mode MMD

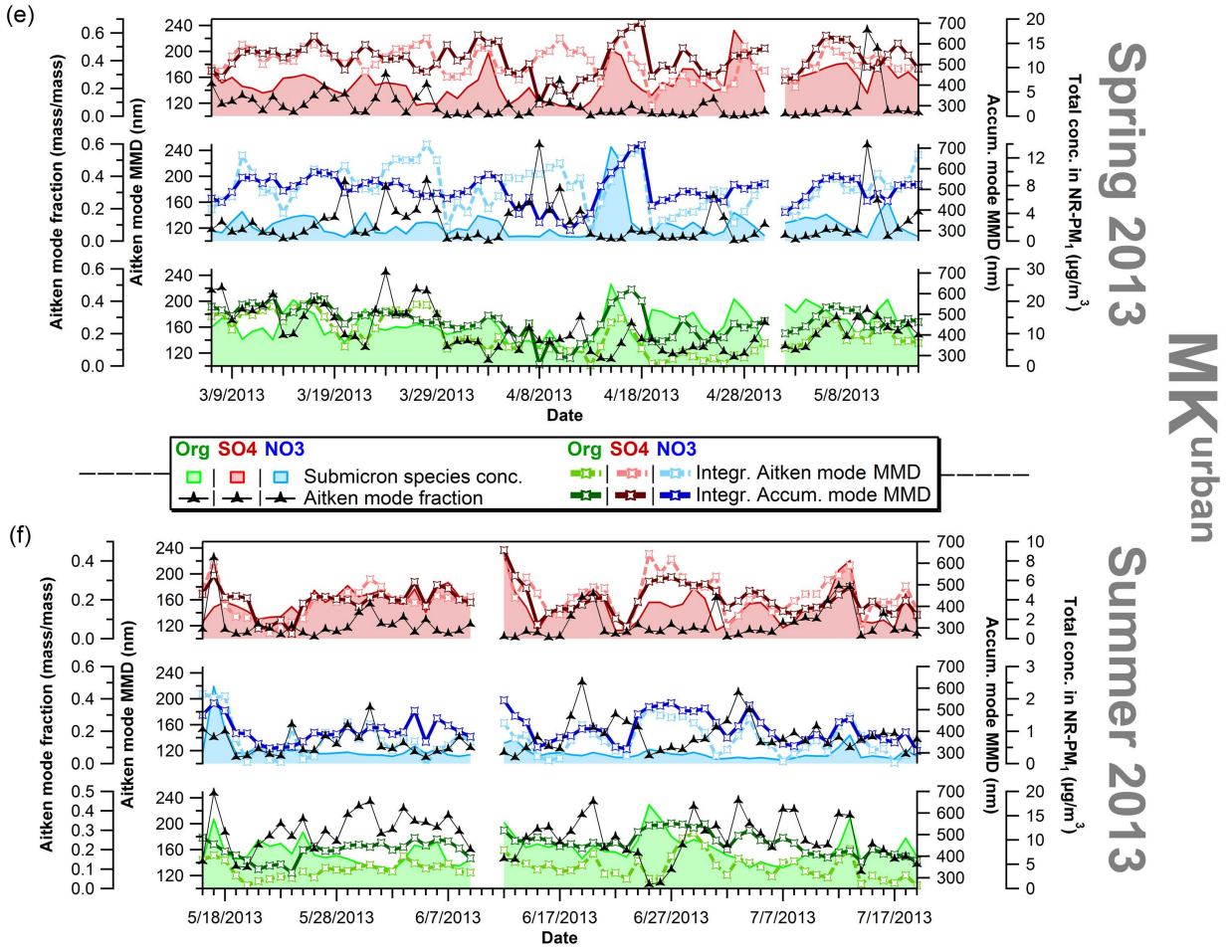

Figure S16. Time series of mass median diameters of Aitken and accumulation modes at the suburban HKUST supersite in four seasons in 2011-2012 (a-d) and the urban Mong Kok site in 2013 (e-f), total species mass concentrations are based on V-mode measurements.

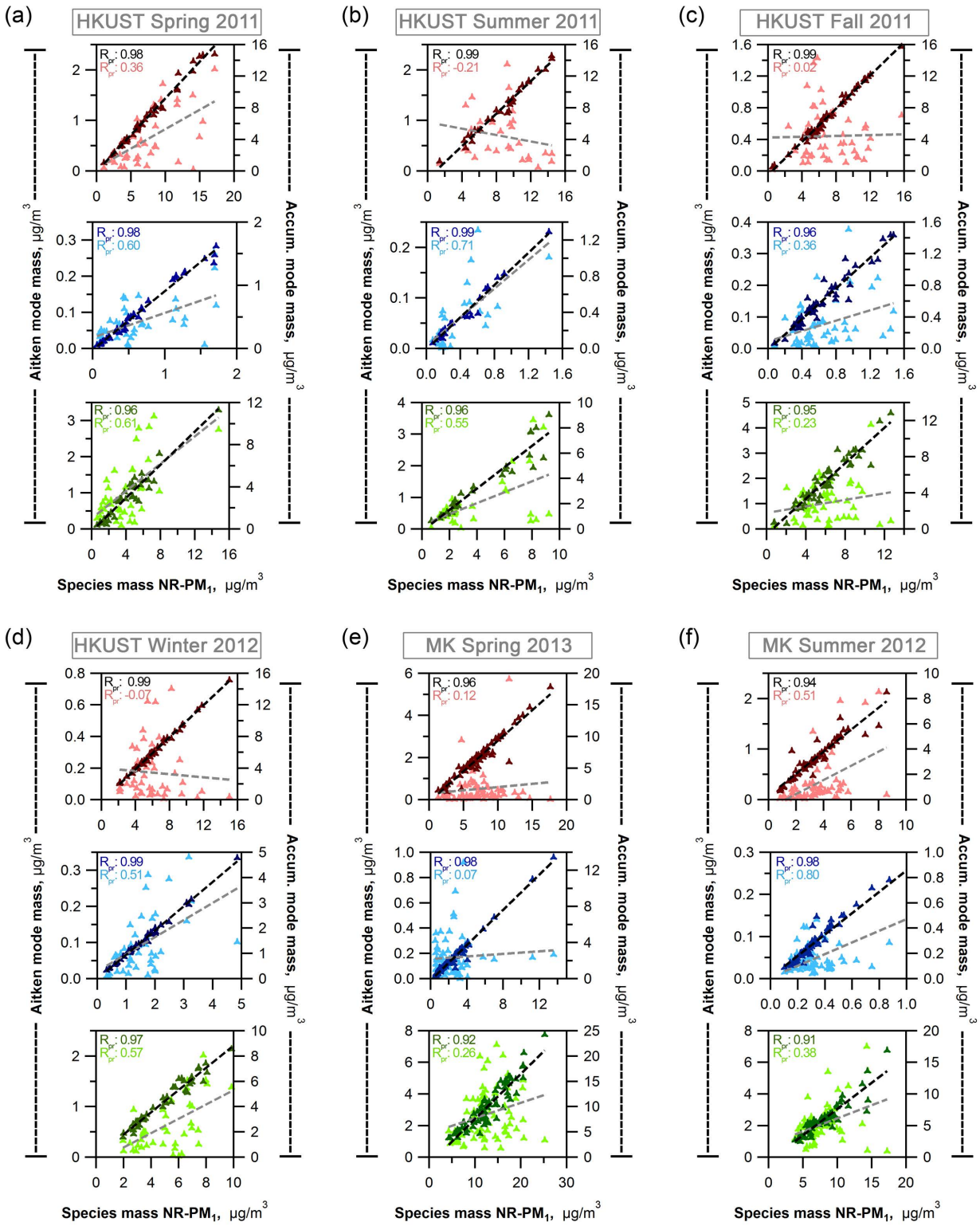

Figure S17. Scatter plot of Aitken and accumulation mode mass concentrations and total species concentrations in NR-PM_1 (AMS V-mode at the HKUST supersite (a-d) and the Mong Kok urban site (e-f)

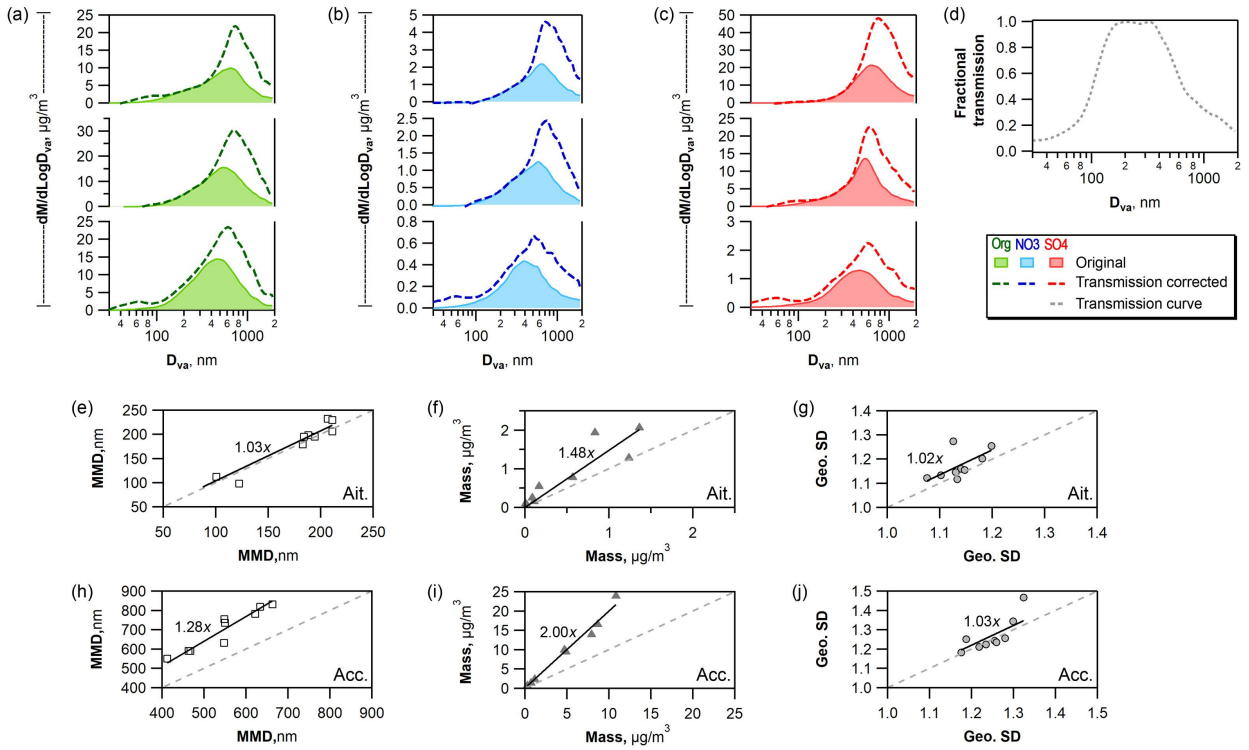

Figure S18. Examples of 24h size distributions from the fall season HKUST dataset for (a) organics, (b) nitrate, (c) sulfate; *original size distributions shaded and lens transmission corrected size distributions up to 2.0µm as hashed lines;* (d) applied lens transmission curve from Liu et al., 2007 with interpolation between data points and a linearly flattening tail between 1.1 and 2.0 *µm*; scatter plots of fit parameters from bimodal peak fits for the Aitken mode (e-g) and the accumulation mode (h-j); *original size distributions on x-axis and lens transmission corrected size distributions on y-axis.*

References

Allan, J. D., Jimenez, J. L., Williams, P. I., Alfarra, M. R., Bower, K. N., Jayne, J. T., Coe, H., and Worsnop, D. R.: Quantitative sampling using an Aerodyne aerosol mass spectrometer - 1. Techniques of data interpretation and error analysis, J. Geophys. Res. Atmos., 108, https://doi.org/4090 10.1029/2002jd002358, 2003.

Canagaratna, M. R., Jayne, J. T., Jimenez, J. L., Allan, J. D., Alfarra, M. R., Zhang, Q., Onasch, T. B., Drewnick, F., Coe, H., Middlebrook, A., Delia, A., Williams, L. R., Trimborn, A. M., Northway, M. J., DeCarlo, P. F., Kolb, C. E., Davidovits, P., and Worsnop, D. R.: Chemical and microphysical characterization of ambient aerosols with the aerodyne aerosol mass spectrometer, Mass Spectrom. Rev., 26, 185-222, https://doi.org/10.1002/mas.20115, 2007.

DeCarlo, P. F., Slowik, J. G., Worsnop, D. R., Davidovits, P., and Jimenez, J. L.: Particle morphology and density characterization by combined mobility and aerodynamic diameter measurements. Part 1: Theory, Aerosol Sci. Technol., 38, 1185-1205, https://doi.org/10.1080/027868290903907, 2004.

DeCarlo, P. F., Kimmel, J. R., Trimborn, A., Northway, M. J., Jayne, J. T., Aiken, A. C., Gonin, M., Fuhrer, K., Horvath, T., Docherty, K. S., Worsnop, D. R., and Jimenez, J. L.: Field-deployable, high-resolution, time-of-flight aerosol mass spectrometer, Anal. Chem., 78, 8281-8289, https://doi.org/10.1021/ac061249n, 2006.

Drewnick, F., Hings, S. S., DeCarlo, P., Jayne, J. T., Gonin, M., Fuhrer, K., Weimer, S., Jimenez, J. L., Demerjian, K. L., Borrmann, S., and Worsnop, D. R.: A new time-of-flight aerosol mass spectrometer (TOF-AMS) - Instrument description and first field deployment, Aerosol Sci. Technol., 39, 637-658, https://doi.org/10.1080/02786820500182040, 2005.

Gill, P. E., Murray, W., and Wright, M. H.: The Levenberg-Marquardt method, in: Practical optimization, Academic Press, London, 1981.

Jayne, J. T., Leard, D. C., Zhang, X. F., Davidovits, P., Smith, K. A., Kolb, C. E., and Worsnop, D. R.: Development of an aerosol mass spectrometer for size and composition analysis of submicron particles, Aerosol Sci. Technol., 33, 49-70, https://doi.org/10.1080/027868200410840, 2000.

Jimenez, J. L., Jayne, J. T., Shi, Q., Kolb, C. E., Worsnop, D. R., Yourshaw, I., Seinfeld, J. H., Flagan, R. C., Zhang, X. F., Smith, K. A., Morris, J. W., and Davidovits, P.: Ambient aerosol sampling using the Aerodyne Aerosol Mass Spectrometer, J. Geophys. Res. Atmos., 108, 8425, https://doi.org/10.1029/2001jd001213, 2003.

Jimenez, J. L., Decarlo, P., Kimmel, J. R., Huffman, J. A., Ulbrich, I., Dunlea, E., Trimborn, A., Northway, M. J., Jayne, J. T., Aiken, A. C., Gonin, M., Fuhrer, K., Horvath, T., Docherty, K. S., and Worsnop, D. R.: Development and application of a high-resolution time-of-flight aerosol mass spectrometer, Abstracts of Papers of the American Chemical Society, 233, 590-590, 2007.

Lee, B. P., Li, Y. J., Yu, J. Z., Louie, P. K. K., and Chan, C. K.: Characteristics of submicron particulate matter at the urban roadside in downtown Hong Kong-Overview of 4 months of continuous high-resolution aerosol mass spectrometer measurements, J. Geophys. Res. Atmos.,, 120, 7040-7058, https://doi.org/10.1002/2015jd023311, 2015.

Li, Y. J., Lee, B. P., Su, L., Fung, J. C. H., and Chan, C. K.: Seasonal characteristics of fine particulate matter (PM) based on high-resolution time-of-flight aerosol mass spectrometric (HR-ToF-AMS) measurements at the HKUST Supersite in Hong Kong, Atmos. Chem. Phys., 15, 37-53, https://doi.org/10.5194/acp-15-37-2015, 2015.

Slowik, J. G., Stainken, K., Davidovits, P., Williams, L. R., Jayne, J. T., Kolb, C. E., Worsnop, D. R., Rudich, Y., DeCarlo, P. F., and Jimenez, J. L.: Particle morphology and density characterization by combined mobility and aerodynamic diameter measurements. Part 2: Application to combustion-generated soot aerosols as a function of fuel equivalence ratio, Aerosol Sci. Technol., 38, 1206-1222, https://doi.org/10.1080/027868290903916, 2004.